This is the peer reviewed version of the following article: Yang, X. L., Yue, L., Yu, Y., Liu, B. A., Dang, J. S., Sun, Y. H., Zhou, G. J., Wu, Z. X., Wong, W.-Y., Strategically Formulating Aggregation-Induced Emission-Active Phosphorescent Emitters by Restricting the Coordination Skeletal Deformation of Pt(II) Complexes Containing Two Independent Monodentate Ligands. Adv. Optical Mater. 2020, 8, 2000079, which has been published in final form at https://doi.org/10.1002/adom.202000079. This article may be used for non-commercial purposes in accordance with Wiley Terms and Conditions for Use of Self-Archived Versions.

Strategically Formulating Aggregation-Induced Emission (AIE)-active Phosphorescent Emitters by Restricting the Coordination Skeletal Deformation of Pt(II) Complexes Containing Two Independent Monodentate Ligands

Xiaolong Yang, Ling Yue, Yue Yu, Boao Liu, Jingshuang Dang, Yuanhui Sun, Guijiang Zhou, Zhaoxin Wu,* and Wai-Yeung Wong**

Dr. X. L. Yang, Dr. L. Yue, Dr. Y. Yu, B. A. Liu, Dr. Y. H. Sun, Prof. G. J. Zhou
Department of Chemistry, School of Science
MOE Key Laboratory for Nonequilibrium Synthesis and Modulation of Condensed Matter
Xi'an Jiaotong University, Xi'an 710049, P. R. China
E-mail: zhougj@mail.xjtu.edu.cn

Dr. X. L. Yang, B. A. Liu, Prof. W.-Y. Wong
Department of Applied Biology and Chemical Technology
The Hong Kong Polytechnic University
Hung Hom, Hong Kong, P. R. China
E-mail: wai-yeung.wong@polyu.edu.hk

Prof. W.-Y. Wong
The Hong Kong Polytechnic University Shenzhen Research Institute
Shenzhen 518057, P. R. China

Dr. J. S. Dang
School of Chemistry and Chemical Engineering
Shaanxi Normal University, Xi'an 710119, P. R. China

Prof. Z. X. Wu
Key Laboratory for Physical Electronics and Devices of the Ministry of Education
School of Electronic and Information Engineering
Xi'an Jiaotong University, Xi'an 710049, P. R. China
E-mail: zhaoxinwu@mail.xjtu.edu.cn

Abstract

Aggregation-induced emission (AIE)-active phosphorescent emitters have intrinsic advantages in time-gated imaging/sensing and improving the electroluminescent efficiencies of organic light-emitting devices (OLEDs). However, compared with the very prosperous and fruitful developments of AIE-active fluorescent emitters and related working mechanisms, the progresses on AIE-active phosphorescent emitters and associated AIE mechanisms are still relatively slow. Herein, we report on the AIE properties of a series of phosphorescent Pt(II) complexes with two monodentate ligands. Compared with the conventional rigid Pt(II) complexes bearing two bidentate ligands or one tri-/tetradentate ligand, the incorporation of two monodentate ligands provides the resulting Pt(II) complexes more room to deform their coordination skeletons from the square-planar geometry in the ground state to the quasi-tetrahedral configuration in the excited state, causing poor solution emissions. In doped films and aggregate states, intense emissions are observed for these Pt(II) complexes. The as-fabricated solution-processed OLED device exhibits an impressively high external quantum efficiency of 21.7%. This study provides an effective way to develop excellent AIE-active phosphorescent emitters.

1. Introduction

Aggregation-induced emission (AIE) refers to the extraordinary phenomenon that an emitter showing no or weak emission in a dilute solution can be highly emissive in the aggregate state or solid state.[1] Since this concept was firstly proposed by Tang et al. in 2001, research works in the AIE field have been flourishing, and tremendous AIE luminogens (AIEgens) or AIE-active emitters have been developed and successfully applied as functional materials in optoelectronic devices or probes in cell imaging and chemical sensing.[2-8] Along with the development of various functional AIE-active emitters, the related working mechanisms have also been proposed. The generally accepted theories, namely, restriction of intramolecular rotations (RIR) and restriction of intramolecular vibrations (RIV) have been unified as restriction of intramolecular motions (RIM, RIM = RIR+RIV), which can interpret most AIE phenomena.[5] Other AIE mechanisms are proposed on the basis of their properties in the excited states, such as the restriction of π-bond twist,[9, 10] suppression of Kasha's rule[11, 12], restriction of access to the dark state,[13] through-space conjugation,[14, 15] and confinement of structural distortions including the chemical bond elongation, plane distortion, and cluster distortion.[16-18] However, studies of materials as well as working mechanisms are mostly focused on AIE-active fluorescent emitters. Compared with the short lifetimes in the nanosecond scale for fluorescent emitters, the much longer lifetimes in the microsecond level endow the phosphorescent analogues with the advantages in time-gated imaging or sensing, that is, the long-lived phosphorescence signal can be used to eliminate the short-lived background fluorescence interference to enhance the signal-to-noise ratios.[19-22] In addition, phosphorescent organometallic complexes usually show larger Stokes shifts which can subdue the detrimental self-quenching effect caused by overlapping between the excitation and emission spectra to improve the measurement accuracy and imaging contrast.[23] Furthermore, in organic light-emitting devices (OLEDs), only ca. 25% electrically generated excitons can be used by the conventional fluorescent molecules to emit light, whereas the phosphorescent organometallic complexes can fully utilize all the electrically generated excitons for emissions and thence boost the electroluminescent efficiencies.[24, 25] Although some phosphorescent organometallic complexes, such as cyclometalated Ir(III) and Pt(II) complexes, have been brilliantly designed to possess impressive AIE properties for chemosensing,[26, 27] bioimaging,[28-30] and OLEDs,[31-35] both the material type and the applications of phosphorescent AIE-active emitters are still lagging behind as compared with those of the organic fluorescent AIE-active emitters.[1, 36-38] Based on the general RIM mechanism, the effective tactic used to endow the fluorescent emitters with AIE properties is to introduce the intramolecular motions (rotation and vibration) by incorporating aromatic groups as free rotors to relax the excited state via non-radiative decays,[8] and this tactic has also be grafted to design AIE-active organometallic complexes.[26, 29, 32, 33, 39-41] However, unlike the pure organic emitters, the emissions of organometallic complexes often involve the significant participation of the metal-to-ligand charge transfer (MLCT) transitions, which can enhance the phosphorescence.[42, 43] Hence, many organometallic complexes containing free rotors can still be highly emissive in solutions,[44-49] indicating that the strategy of designing AIE-active organometallic complexes by purely incorporating rotatable substituents into the ligands is not good enough. On the other hand, due to the long emission lifetimes, severe triplet-triplet annihilation (TTA) will occur at high concentrations or aggregate states to quench the phosphorescence of organometallic complexes.[50] Therefore, it is still challenging and urgently needed for a more effective strategy to develop AIE-active phosphorescent emitters.

In contrast to the common phosphorescent emitters, such as the Ir(III) complex *fac*-tris(2-phenylpyridine)iridium(III) [$Ir(ppy)_3$] which usually encounters the severe TTA effect at high concentration or aggregate state,[51, 52] cyclometalated Pt(II) complexes may prevent the strong concentration quenching because their square-planar structure can facilitate strong molecular stacking to induce the bright excimer or metal-metal-to-ligand charge-transfer (MMLCT) emissions, thereby avoiding the high concentration or aggregation quenching.[53-57] Therefore, among all phosphorescent emitters, cyclometalated Pt(II) complexes have great potential to exhibit excellent AIE properties. The only question is on how to reasonably design the chemical structures of Pt(II) complexes. As mentioned before, the emissions of organometallic complexes significantly involve the contribution of the metal centers. Thus, the manipulation of the coordination spheres around the Pt center has the ability to control the emission properties of Pt(II) complexes. For example, enhancement of the molecular rigidity around the Pt center by replacing a bidentate ligand with a tridentate cyclometalating ligand can dramatically improve the solution photoluminescence quantum yields (PLQY) from 0.02

for the bidentate complex to 0.80 for the tridentate complex.[58] Rigid Pt(II) complexes bearing tetradentate ligands often display considerably high PLQYs in solutions because the intramolecular motions and distortions related to the non-radiative decays can be effectively suppressed.[59-62] These results imply that adopting rigid structure is not suitable for designing AIE-active Pt(II) complexes. Therefore, on the contrary, reduction of the molecular rigidity will provide the room for intramolecular motions and distortions. Theoretical calculation results reported by Yam et al. showed that the monodentate ligands of tridentate Pt(II) complexes would slightly bend away from the plane containing the tridentate ligand and the Pt center in the excited states to favor the non-radiative decay from the triplet metal-centered state (^{3}MC).[63] Huang et al. designed a series of bidentate Pt(II) complexes based on 2-phenylpyridine-type ligands and Schiff-base ligands.[17] In the T_1 state, the Schiff-base ligands bent along the Pt-N (in Schiff-base ligand) single bond to distort the chelating six-membered cycle between Pt and Schiff-base ligands, resulting in very weak emission in solutions. These results suggest that structural distortions of Pt(II) complexes in the excited state may lead to emissions quenching in solution. Therefore, in order to reduce the molecular rigidity and provide more space for the chemical structure to distort in the excited state, a series of Pt(II) complexes containing two independent monodentate ligands were designed and synthesized (Figure 1). In our initial thought, the two monodentate ligands could not only act as rotors, but also play the key role to unlock the structural distortions, and thus the resulting Pt(II) complexes would display no or weak emission in solutions due to the intramolecular rotation and structural distortion. These Pt(II) complexes indeed exhibited very weak emissions with PLQYs less than 0.02 in CH_2Cl_2 solutions. However, theoretical calculation results showed that the rotation angle changes of the two monodentate ligands were much smaller than the dihedral angle changes around the Pt center in the excited states, demonstrating a much larger amplitude of the structural distortions than that of the ligand rotations. Actually, the coordination skeleton around the Pt center has been distorted from the planar configuration in the ground state to the quasi-tetrahedron configuration in the excited state. Therefore, the coordination skeletal deformation would be more responsible for the solution quenching. In the aggregate or solid state, these Pt(II) complexes were highly emissive mainly because of the physical restriction of the coordination skeletal deformation, manifesting their excellent AIE properties. To further increase the PLQY in the solid state, strong field ligands, i.e., alkynyl ligands, were used to raise the *d-d* transition energy levels and thus decrease the non-radiative decay from the ^{3}MC state. Accordingly, the PLQYs of the doped PMMA films were improved up to 0.8. Therefore, solution-processed OLEDs could display excellent device performance with the best external quantum efficiency (EQE), current efficiency (CE), and power efficiency (PE) of 21.7%, 61.9 cd A^{-1}, and 54.8 lm W^{-1}, respectively, which were among the highest efficiencies reported for doped solution-processed OLEDs utilizing AIE-active phosphorescent emitters. This work proposes a possible AIE mechanism, namely, restriction of coordination skeletal deformation (RCSD), for Pt(II) complexes containing two independent monodentate ligands, which will allow the effective design of high performance AIE-active phosphorescent emitters.

2. Results and Discussion

The AIE-active Pt(II) complexes were synthesized in three simple steps. As shown in Figure 1 and Figure S1 (see Supporting Information), cyclometalated Pt(II) μ-chloro-bridged dimer was firstly obtained by refluxing K_2PtCl_4 with 2-phenylpyridine ligand in a mixture of 2-ethoxyethanol and H_2O (v/v, 3:1),[64] and then the dimer and the monodentate pyridine ligand were stirred in a N_2 atmosphere at 45 °C to give the Cl-containing intermediate complex **PyCl**.[65] Finally, **PyCl** was reacted with a series of alkynyl ligands in an alkaline environment to give the target products with high yields up to 91%. These Pt(II) complexes were fully characterized by NMR (Figure S2 and S3) and high resolution mass spectrometry (Figure S4 and S5). The thermal stability of these Pt(II) complexes investigated by the thermogravimetric analysis showed that the thermal decomposition temperatures (T_d) were in the range from 179 to 247 °C (Table 1), which were high enough for solution-processable applications. It appears that the Pt(II) complex with a larger alkynyl ligand somehow could show higher thermal stability, which was also observed for dendritic carbazole-containing alkynylplatinum(II) complexes.[46]

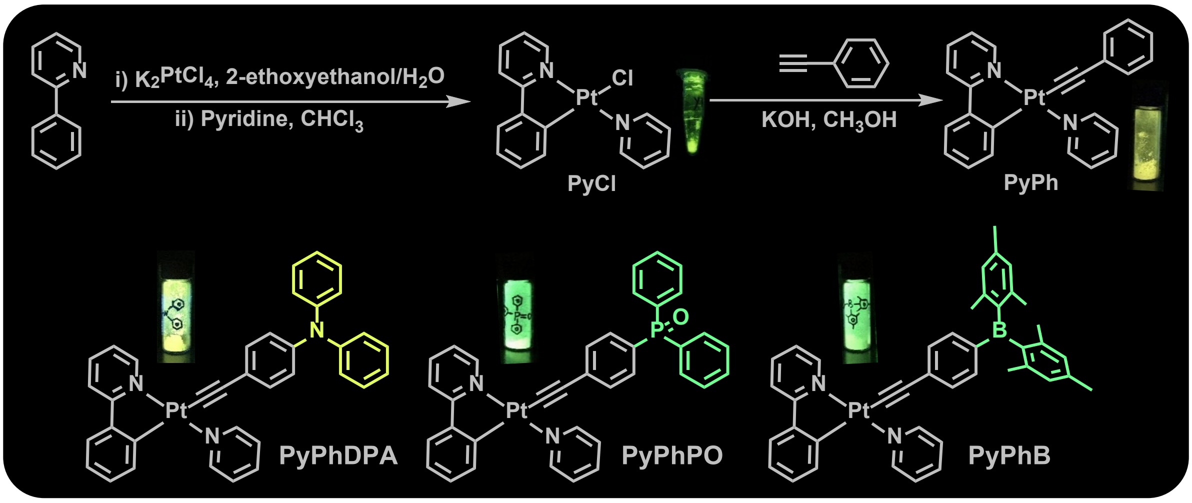

Figure 1. Synthetic routes for the AIE-active Pt(II) complexes containing two monodentate ligands (Inset: Photos of the as-prepared Pt(II) complexes as powders taken under the illumination of 365 nm UV light).

Table 1. Key photophysical, thermal, and energy level data for the AIE-active Pt(II) complexes.

	λ_{abs}[a] [nm]	λ_{em}[b] [nm](τ) Soln./Film	PLQY[b] Soln./Film	k_r ($\times 10^5$ s^{-1})[c] Soln./Film	k_{nr} ($\times 10^5$ s^{-1})[c] Soln./Film	T_d [°C]	HOMO/ LUMO[d] [eV]
PyCl	253, 386	423 (1.1 ns), 485 (0.06 µs) /484 (1.99 µs)	0.016/0.54	2.7/164	2.7/2.3	225	–5.33/–2.39
PyPh	263, 295, 390	422 (1.5 ns), 487 (0.14 µs) /488 (2.90 µs)	0.008/0.29	0.6/70.9	1.0/2.4	179	–5.00/–2.18
PyPhDPA	259, 323, 402	426 (2.0 ns), 489 (0.06 µs) /494 (2.46 µs)	0.020/0.56	3.3/163	2.3/1.8	205	–4.83/–2.06
PyPhPO	260, 307, 388	424 (6.6 ns), 486 (0.13 µs) /490 (2.72 µs)	0.002/0.80	0.2/76.8	2.9/0.7	188	–5.14/–2.27
PyPhB	254, 353, 419	427 (6.2 ns), 506 (0.34 µs) /503 (2.52 µs)	0.008/0.65	0.2/29.2	2.6/1.4	247	–5.11/–2.33

[a] In CH_2Cl_2 at room temperature. [b] In CH_2Cl_2 solution (Soln.) at ca. 2×10^{-5} mol L^{-1} excited with the 350 nm UV light and PMMA film doped with ca.1.0 wt% Pt(II) complex at room temperature (The corresponding lifetimes τ are given in parentheses). [c] Radiative decay rate constant k_r and non-radiative decay rate constant k_{nr} were calculated according to k_r = PLQY/τ and k_{nr} = (1–PLQY)/τ. [d] Energy levels of HOMOs (E_{HOMO}) were determined from the onset of oxidation potentials (E_{ox}) according to $E_{HOMO} = -(E_{ox} + 4.8)$ eV and energy levels of LUMOs (E_{LUMO}) were determined from E_{HOMO} and optical band gaps (E_{gap}) according to $E_{LUMO} = E_{HOMO} + E_{gap}$.

The UV–vis absorptions spectra of these Pt(II) complexes were measured in CH_2Cl_2 solutions at room temperature. As shown in Figure 2a, all complexes showed intense structured absorption bands at around 250 nm, which were assigned to the spin-allowed ligand-centered (LC) $\pi \rightarrow \pi^*$ transitions of 2-phenylpyridine ligand.[64] Except for **PyCl**, strong absorption bands in the range of 290-350 nm were observed for these alkynyl ligand-containing Pt(II) complexes, which mainly resulted from the spin-allowed LC $\pi \rightarrow \pi^*$ transitions of the corresponding alkynyl ligands.[66] In the low energy range of 375-450 nm, weak and broad absorption bands were detected for both the Cl-containing and alkynyl ligand-containing Pt(II) complexes, probably due to the metal-to-ligand charge transfer (MLCT) and ligand-to-ligand charge transfer (LLCT) transitions.[67] As the inset in Figure 2a illustrated, slightly red-shifted low energy absorptions were realized by substituting the Cl^- ligand with alkynyl ligands because the alkynyl ligand possessed stronger chelating field than the Cl^- ligand.[67] Furthermore, compared with that of **PyPh**, the low energy absorption of **PyPhDPA** which had an electron-donating substituent [diphenylamino (DPA)] attached on the phenylacetylene ligand was red-shifted, whereas that of **PyPhPO** with an electron-withdrawing substituent [diphenylphosphino oxide (PO)] was blue-shifted. It was reasonable that the electron-donating substituent on the alkynyl ligand would raise the energy of the $d\pi$(Pt) and π(alkynyl ligand) orbitals to lower the energy level of the charge transfer (CT) states, whereas electron-withdrawing substituents would cause the opposite effect.[67] Complex **PyPhB** showed relatively stronger and more red-shifted absorptions even though it had an electron-withdrawing substituent [dimesitylboryl (B)] attached on the phenylacetylene ligand, suggesting different CT patterns in **PyPhB** because of the strong π-electron accepting ability of the dimesitylboryl group.[44] The above results were further supported by the cyclic voltammetry (CV) investigation and theoretical calculations (see below).

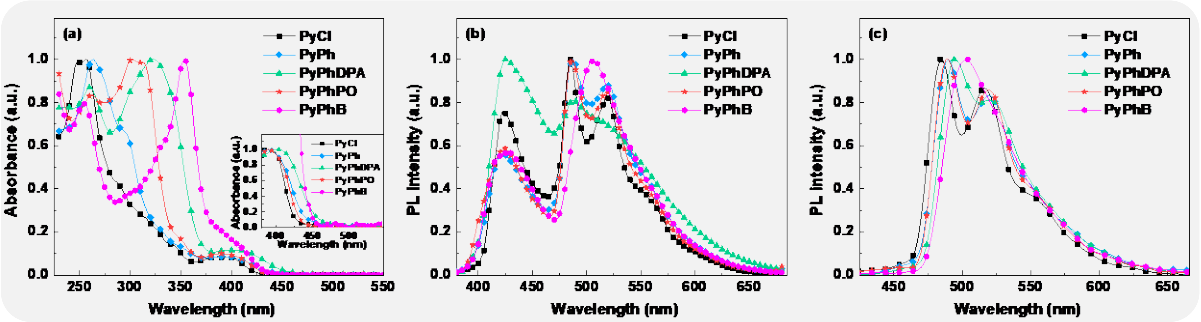

Figure 2. a) UV-vis absorptions of these Pt(II) complexes in CH_2Cl_2, b) PL spectra of these Pt(II) complexes in CH_2Cl_2, and c) PL spectra of doped PMMA films at the doping level of ca. 1.0 wt%.

To have a better understanding on the electronic structures and absorption behaviors of these Pt(II) complexes, natural transition orbital (NTO) analysis using the density functional theory (DFT) and time-dependent DFT (TD-DFT) were carried out. The distributions of hole (H) and particle (P) orbitals are depicted in Figure 3, while the related data are summarized in Table 2. The calculated results showed that hole → particle (H → P) transitions made decisive contributions to the excited states. For **PyCl**, its hole orbital was mainly located on the Pt center, the chelated phenyl ring, and the Cl^- ligand, while the particle orbital was mainly contributed by the 2-phenylpyridine ligand (PPy) and the monodentate pyridine ligand (Py), and thus the low energy absorption of **PyCl** could be assigned to a mixture of LC [π(PPy) → π^*(PPy)], MLCT [dπ(Pt) → π^*(PPy) and π^*(Py)], and LLCT [p_{Cl} → π^*(PPy) and π^*(Py)] transitions. By replacing the Cl^- ligand with alkynyl ligands (L-alkynyl), the particle orbital distribution behaviors of **PyPh**, **PyPhDPA**, and **PyPhPO** were similar to that of **PyCl**. However, alkynyl ligands made more contributions than the Cl^- ligand to the hole orbitals of the pertinent complexes. In addition, the functional substituents had a notable effect on the contribution from alkynyl ligands to the hole orbitals. For example, the electron-donating moiety in **PyPhDPA** could increase the contribution from the alkynyl ligand to the hole orbital, while the electron-withdrawing substituent in **PyPhPO** had the opposite influence. Therefore, the low energy absorptions of **PyPh**, **PyPhDPA**, and **PyPhPO** were assigned to the mixture of LC [π(PPy) → π^*(PPy)], MLCT [dπ(Pt) → π^*(PPy) and π^*(Py)], and LLCT [π(alkynyl ligand) → π*(PPy) and π*(Py)] transitions. The excitation of **PyPhB** had two pairs of hole to particle transitions with the contribution percentages of 81.14% (H1 → P1) and 15.54% (H2 → P2), respectively. Except that the PPy made more contribution to both H1 and P1 of **PyPhB**, the H1 → P1 transition of **PyPhB** was similar to that of **PyPhPO**, and thus the H1 → P1 transition was mainly assigned to LC [π(PPy) → π*(PPy)] mixed with some MLCT [dπ(Pt) → π*(PPy) and π*(Py)], and LLCT [π(alkynyl ligand) → π*(PPy) and π*(Py)] transitions. The great contribution (> 83%) from the alkynyl ligand to both H2 and P2 revealed the dominant LC [π(alkynyl ligand) → π*(alkynyl ligand)] character of the H2 → P2 transition. The unexpected two pairs of hole to particle transitions might be related to the strong π-electron accepting ability of the dimesitylboryl group, thereby leading to the special absorption behavior of **PyPhB**. The calculation results were in good agreement with the experimental observations.

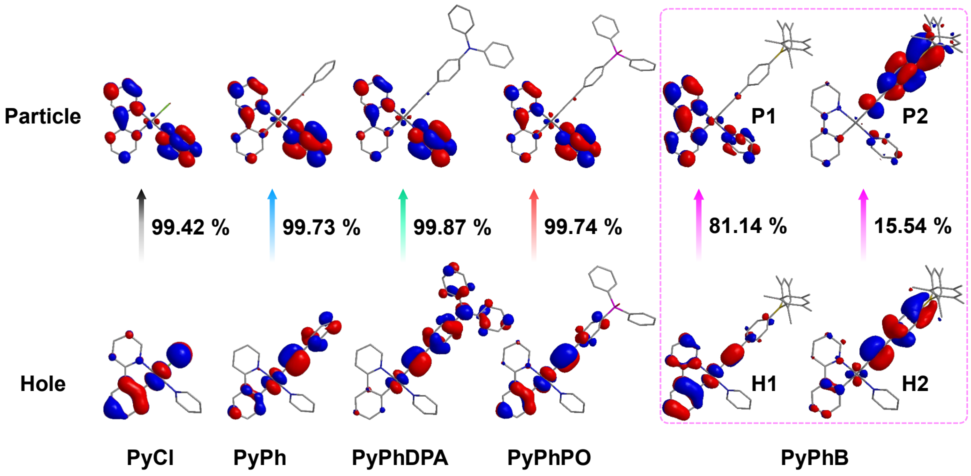

Figure 3. NTO hole and particle orbital distributions of these Pt(II) complexes.

Table 2. NTO analysis results for these Pt(II) complexes.

	NTOs	Contribution from Pt and ligands to NTOs (%)			
PyCl		**Pt**	**PPy**	**Py**	**Cl**
	P	4.06	48.66	46.73	0.55
	H	41.10	31.41	0.12	27.37
PyPh		**Pt**	**PPy**	**Py**	**L-alkynyl**
	P	3.41	29.96	65.65	0.98
	H	23.53	13.05	0.55	62.87

PyPhDPA		**Pt**	**PPy**	**Py**	**L-alkynyl**
	P	3.38	29.85	65.42	1.35
	H	9.69	4.16	0.49	85.66
PyPhPO		**Pt**	**PPy**	**Py**	**L-alkynyl**
	P	3.69	33.07	62.47	0.77
	H	30.71	21.11	0.15	48.03
PyPhB		**Pt**	**PPy**	**Py**	**L-alkynyl**
	P1	5.18	77.55	13.94	3.33
	H1	24.48	52.15	0.09	23.28
	P2	1.02	7.00	5.21	86.77
	H2	3.93	11.70	0.41	83.96

The emission properties of these Pt(II) complexes were studied in both CH_2Cl_2 solutions and doped poly(methyl methacrylate) (PMMA) films at the doping level of ca. 1 wt %. As shown in Figure 2b, all these Pt(II) complexes showed two main emission bands in CH_2Cl_2 solutions. The high-energy emissions with peaks at around 425 nm showed the decay lifetimes of only about a few nanoseconds (Table 1), indicating their fluorescence characteristics. In the low energy range from 480 to 560 nm, these Pt(II) complexes exhibited emissions with the observed lifetimes prolonged to 0.37 μs. The much longer lifetimes and large Stokes shifts implied that these low-energy emissions were of triplet parentage. Among these Pt(II) complexes, **PyCl**, **PyPh**, and **PyPhPO** showed clearly structured photoluminescence (PL) spectra, indicating their phosphorescent emissions probably originated from the ^{3}CT/^{3}LC excited states.[42] As shown in Figure 3, the phenyl rings chelated to the Pt centers in **PyCl**, **PyPh**, and **PyPhPO** made notable contributions to both hole and particle orbitals, confirming the presence of ^{3}LC [π(chelated phenyl rings) → π*(chelated phenyl rings)] transitions. As for **PyPhDPA** and **PyPhB**, their PL spectra were broad and less structured, suggesting the related phosphorescence mainly resulted from the ^{3}CT excited states.[42] The calculated results showed that **PyPhDPA** possessed an almost completely separated hole and particle orbitals, manifesting the lack of ^{3}LC transitions. Considering the low contribution from the Pt center to the hole orbital, the phosphorescence of **PyPhDPA** should arise from the ^{3}LLCT [π(alkynyl ligand) → π*(PPy) and π*(Py)] transitions mixed with minor ^{3}MLCT features. As for **PyPhB**, the key orbital distributions showed that the dimesitylboryl group caused significant intraligand charge transfer (ILCT) within the alkynyl ligand. Therefore, the phosphorescent emission of **PyPhB** was caused the mixture of ^{3}MLCT/^{3}LLCT/^{3}ILCT transitions. Compared with **PyCl** which exhibited the phosphorescence peak at 485 nm, the alkynyl ligand-containing Pt(II) complexes showed slightly red-shifted phosphorescent emission peaks, which were in agreement with their slightly red-shifted low energy absorptions. In the doped PMMA films, only the low energy emissions were observed, and the PL spectra were similar to the related phosphorescent emissions in the CH_2Cl_2 solutions. In addition, the emission lifetimes of these doped films were prolonged to 2.3-2.9 μs, unambiguously demonstrating their triplet parentage. Importantly, the PLQYs of these Pt(II) complexes were dramatically increased up to 0.80 in the doped PMMA films at a concentration of ca. 1.0 wt%. Based on the PLQYs and corresponding lifetimes, radiative decay rate constant k_r and non-radiative decay rate constant k_{nr} were calculated. Compared with those in solutions, the k_rs were unchanged or increased, while the k_{nr}s were greatly decreased in the solid state, resulting in enhanced emissions. This result was well-expected since these Pt(II) complexes could show intense emissions under the illumination of 365 nm UV light (Figure 1). Besides, no matter whether they were in the solution or solid state, the k_{nr}s of the alkynyl ligand-containing Pt(II) complexes were basically smaller than that of **PyCl**. Generally, the Cl^- ligand is a weak-field ligand, whereas alkynyl ligands are strong-field ligands in the spectrochemical series.[68] With strong-field ligands chelated to the Pt centre, a larger *d-d* ligand-field splitting will be induced to raise the energy level of the *d-d* excited state.[24, 69] As shown in Figure S6, the calculated the *d-d* transition energies were 6.295, 6.339, 6.329, and 6.326 eV for **PyPh**, **PyPhDPA**, **PyPhPO**, and **PyPhB**, respectively, which were significantly higher than that for **PyCl** (6.035 eV). The higher-lying *d-d* excited state can reduce the non-radiative deactivation to benefit the emissions.[67, 70, 71] Therefore, **PyPhDPA**, **PyPhPO**, and **PyPhB** could display higher PLQYs than **PyCl** in the doped films. It was unexpected that **PyPh** somehow showed a relatively higher k_{nr} and thus lower PLQY, suggesting some other non-radiative decay channels in the solid state. Nevertheless, all these Pt(II) complexes could show greatly enhanced PLQYs in the solid states.

The AIE properties were further investigated by measuring their PL spectra in THF/water mixtures (Figure 4 and Figure S7). During the measurements, deionized water was added into the THF solutions with the water fraction (f_w) increased up to 95% (v/v) while keeping the concentration of these Pt(II) complexes unchanged. As shown in Figure 4, the phosphorescent emission of **PyCl** was gradually enhanced by adding water, and the brightest emission was achieved at f_w = 90%, demonstrating the AIE behavior. When f_w was lower than 70%, the emissions of **PyPhDPA**, **PyPhPO**, and **PyPhB** were quite weak and the PL spectra profiles were very similar to those of the emissions in pure THF. However, upon increasing f_w up to 95%, at which point the hydrophobic complexes will significantly aggregate, **PyPhDPA**, **PyPhPO**, and **PyPhB** displayed strong emissions with the intensities of phosphorescence peaks much higher than those of the corresponding fluorescence peaks, confirming their impressive AIE properties. As shown in Figure S8, the PL spectrum profile of **PyPhDPA** in the aggregate state (f_w = 95%) was different from those of **PyPhDPA** in dilute solution as well as 1.0 wt% doped PMMA film. The broad and red-shifted PL spectrum implied the existence of the intermolecular π-π stacking interaction of **PyPhDPA** in aggregate state.[32] Compared with the PL spectra of **PyPhPO** and **PyPhB** in 1.0 wt% doped PMMA, the red-shifted emissions of **PyPhPO** and **PyPhB** at f_w = 95%, respectively, also signified the intermolecular π-π stacking interaction.[32] As for **PyCl**, the obviously enhanced shoulder emissions peaking at 515 and 545 nm suggested that the strong intermolecular interaction was present even at f_w = 70%. The small Cl^- ligand would fail to prevent the molecular aggregation at f_w = 70% since the square-planar Pt(II) complexes usually showed strong tendency to form intermolecular interactions.[72] In contrast, the steric hindrance induced by the bulky alkynyl ligands could reduce the intermolecular interactions to form loose amorphous aggregate of **PyPhDPA**, **PyPhPO**, and **PyPhB**, and thus the non-radiative decay channels could still be active to quench the emissions at f_w < 70%. The different emission enhancement behaviors between the Cl-containing and alkynyl ligand-containing Pt(II) complexes clearly reflected the significant influences exerted by both the strong-field and steric hindrance of alkynyl ligands on the emission properties.

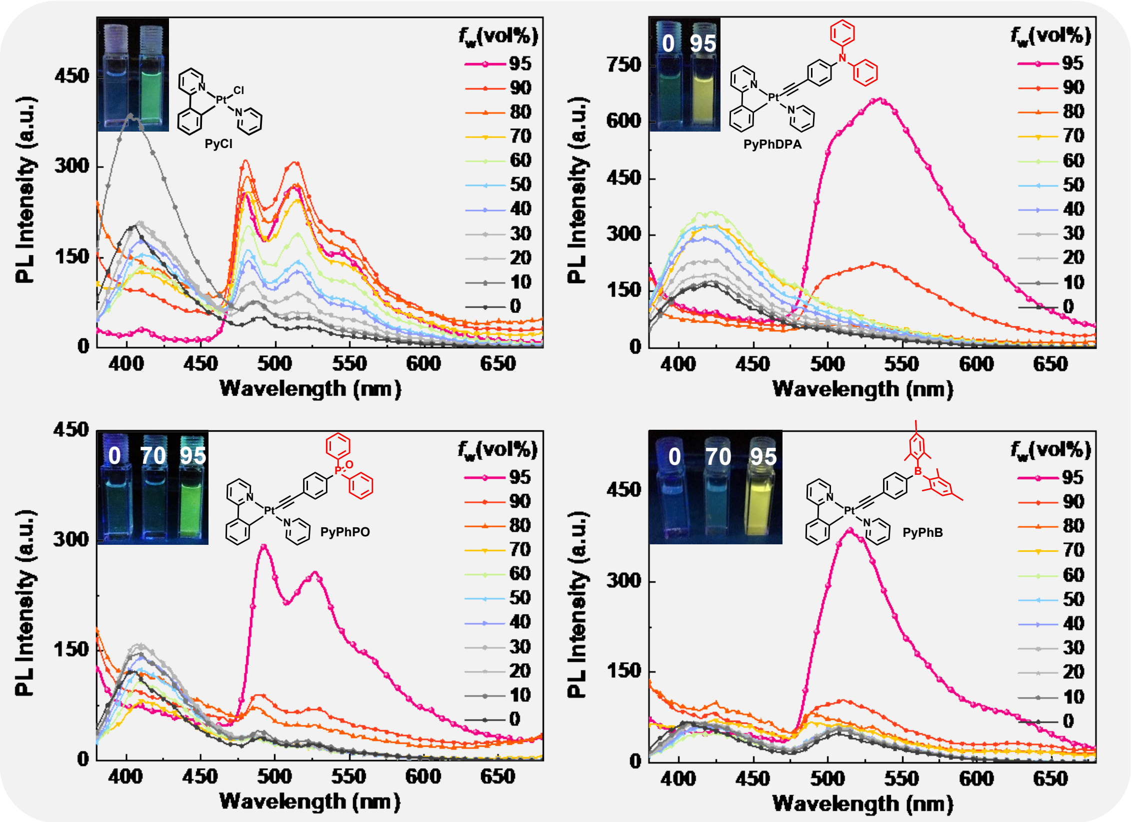

Figure 4. PL spectra of the Pt(II) complexes in THF/water mixtures with different f_w (Inset: Photos of these Pt(II) complexes in THF/water mixtures taken under the illumination of 365 nm UV light).

It has been well-accepted that the intramolecular bond rotations will promote the non-radiative decay to result in rather weak emissions, and the restriction of intramolecular rotation (RIR) in the aggregate state can decrease the non-radiative decay rate to enhance the emissions.[1] Compared with the conventional Pt(II) complexes those bearing two bidentate ligands to form rigid structures and thus to show highly emissive properties in solutions,[64] the two independent monodentate ligands in these newly developed Pt(II) complexes would easily rotate around related single bonds. Based on the RIR mechanism, the weak emissions of these Pt(II) complexes in solutions could be ascribed to the intramolecular bond rotations which facilitated the non-radiative decay to largely lower the PLQYs, and the intense emissions in the aggregate state resulted from the greatly reduced non-radiative decay because of the restriction of the intramolecular bond rotations. However, recent studies showed that the molecular structure in the excited state was crucial for understanding the fundamental working mechanism of AIE-active emitters.[14, 16, 73] Therefore, both the ground and excited geometries of the representative **PyPh** were optimized by CAM-B3LYP and TDA-CAM-B3LYP functionals. As shown in Figure 5, the optimized S_0 geometry of **PyPh** displayed an almost planar structure as the dihedral angles between the plane containing the Pt, N1, and C1 atoms (plane P1) and the plane containing the Pt, N2, and C2 atoms (plane P2) was only 2.7°. The monodentate pyridine ligand is twisted by ca. 54.4° and the alkynyl ligand is twisted by ca. 68.8° against the plane P1. Upon photoexcitation, the monodentate pyridine ligand is rotated with the angle change less than 9°, and the monodentate alkynyl ligand displayed an angle change less than 5°. At the same time, the two monodentate ligands are significantly bent in opposite directions to deform the molecular structure from the planar configuration in the ground state to the quasi-tetrahedron configuration in the S_1 minimum, as supported by the dihedral angles between the plane P1 and the plane P2 of 43.2°. The geometry of the T_1 minimum was back to an almost planar configuration as the dihedral angle between the P1 plane and the P2 plane was reduced to 3.3°. Apparently, replacing one bidentate ligand of the conventional Pt(II) complex with two monodentate ligands could not only provide the room for the two monodentate ligands to rotate freely around the single bonds, but also lift the restriction on the coordination skeletal deformation of the resultant Pt(II) complexes. Moreover, in terms of the degree of rotations, the coordination skeletal deformation was more significant for these Pt(II) complexes. As shown in the linearly interpolated internal coordinate (LIIC) pathways (Figure 6), the S_0/S_1 minimal energy conical intersection (MECI) could be easily reached upon photoexcitation since there was almost no barrier to overcome for the decay from the Frank-Condon point to MECI. Considering the inefficient intersystem crossing (ISC) from S_1 to T_1 supported by the strong fluorescence emission in solutions, the almost barrierless coordination skeletal deformation process to the MECI and thus the provision of the non-radiative decay pathway by an ultrafast internal conversion (IC) was more competitive, leading to the solution-state quenching of the Pt(II) complexes. In the aggregate state, the coordination skeletal deformation would be greatly restricted to increase the energy gap of MECI between S_1 and S_0 and decrease the rate of IC. On the other hand, the planar geometry of T_1 minimum was very similar to that of S_0 and also similar to that of S_1 at the Frank-Condon point, which would benefit the ISC from S_1 to T_1 to promote the emission from the T_1 state. Therefore, phosphorescent emissions of these Pt(II) complexes were greatly enhanced in the aggregate state. Since the AIE-active phosphorescent Pt(II) complexes are still relatively rare and the related AIE mechanism is usually ascribed to the restricted rotational motion in the molecules,[29, 32, 33, 39-41] the restriction of coordination skeletal deformation (RSCD) may be another AIE mechanism specifically for Pt(II) complexes. Because the coordination-unsaturated nature of d^8 transition metal Pt(II) complexes with square-planar structures has the potential to deform its coordination skeleton to the tetrahedral configuration, the proper utilization of two monodentate ligands will not only facilitate the coordination skeletal deformation process during the photoexcitation, but also provide good ways for the vast molecular structure modification to fine-tune the properties of Pt(II) complexes for various applications.

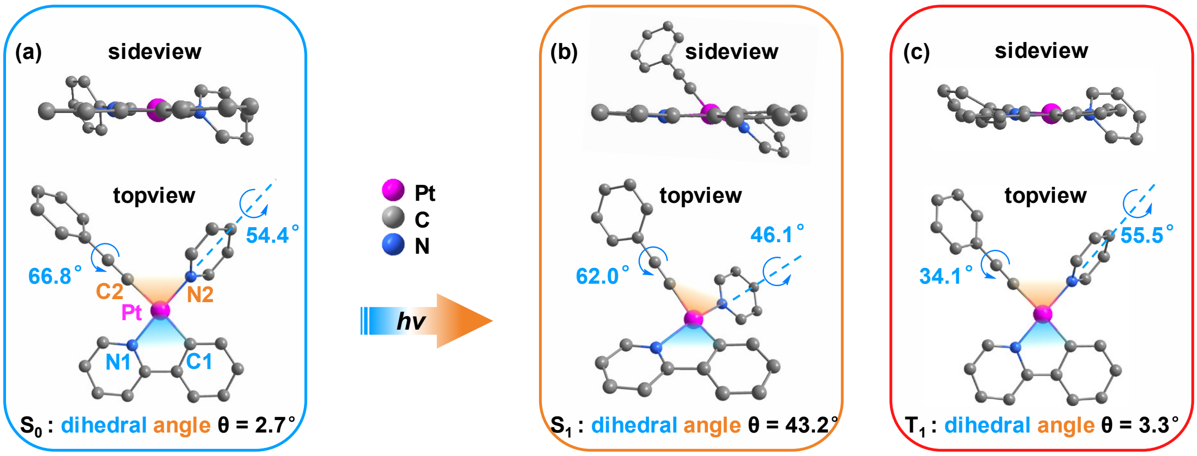

Figure 5. Optimized structures of **PyPh** at a) S_0 minimum, b) S_1 minimum, and c) T_1 minimum (Hydrogen atoms are omitted for clarity).

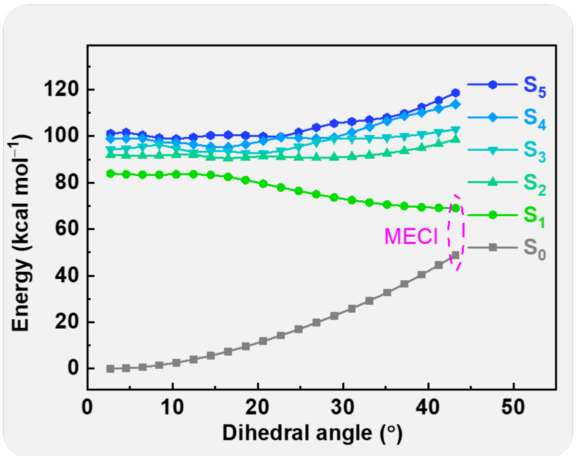

Figure 6. The calculated LIIC pathway from the Frank-Condon point to the MECI of **PyPh**.

The electrochemical properties of these AIE-active Pt(II) complexes were investigated by cyclic voltammetry (CV). As shown in Figure S8, complex **PyCl** showed an irreversible oxidation process with the onset potential (*versus* ferrocene/ferrocenium) of *ca.* 0.53 V, which could be assigned to the oxidation of the segment containing the Pt center and the chelated phenyl ring. Compared with the Cl^- ligand, alkynyl ligands usually show stronger σ-donating ability to destabilize the highest occupied molecular orbital (HOMO) levels.[68] Therefore, a significantly reduced oxidation potential was detected for **PyPh** compared with that of **PyCl**, which was also observed for an alkynyl ligand-containing Pt(II) complex bearing the tridentate 1,3-bis(*N*-butylbenzimidazol-2'-yl)benzene ligand.[66] Due to the strong electron-donating diphenylamino group, the first oxidation potential of **PyPhDPA** was further reduced, and the second quasi-reversible oxidation wave was likely caused by the oxidation of the electron-donating diphenylamino moiety. These results implied that the first oxidation processes mainly occurred at the alkynyl ligands.[66] The assignment was reasonable because the alkynyl ligands made significant or even dominant contribution to the hole orbitals (Figure 3 and Table 2). Therefore, **PyPhPO** and **PyPhB** also showed irreversible oxidation processes with the onset potentials less positive than **PyCl**. During the cathodic scan, no reduction waves were detected for **PyCl**, **PyPh**, **PyPhDPA**, and **PyPhPO**. However, **PyPhB** exhibited a notable irreversible reduction wave at ca. –2.04 V. As the calculation results suggested (Figure 3 and Table 2), the H2 → P2 transition of **PyPhB** significantly involved the dimesitylboryl group because of the strong π-accepting ability, and thus the notable reduction wave could be possibly caused by the reduction of the dimesitylboryl group. The observation of this notable reduction wave also suggested the improved electron injection/transport property of **PyPhB** with respect to other alkynyl ligand-containing Pt(II) complexes. Overall, the electrochemical property investigations demonstrated that the redox behaviors of these AIE-active Pt(II) complexes could be feasibly adjusted by substituting the alkynyl ligands with strong electron-donating or π-accepting groups. This strategy would benefit the performance of the resulting Pt(II) complexes in practical applications.

Because of their high PLQYs in the solid-state, good thermal stability, and interesting redox behaviors, **PyPhDPA**, **PyPhPO**, and **PyPhB** were selected as emitters to evaluate their electroluminescence (EL) performance. The prototype devices were fabricated by the solution-processed method with the conventional device configuration of indium tin oxide (ITO)/poly(ethylenedioxythiophene):poly(styrene sulfonic acid) (PEDOT:PSS) (45 nm)/8 wt% Pt emitter: 4,4′,4″-tri(*N*-carbazolyl)triphenylamine (TCTA) (30 nm)/1,3,5-tris(*N*-phenylbenzimidazole-2-yl)benzene (TPBI) (45 nm)/LiF (1 nm)/Al (100 nm), in which PEDOT:PSS, TCTA, and TPBI functioned as the hole-transporting, host, and electrontransporting materials, respectively (Figure 7). The EL performance characteristics of these devices based on **PyPhDPA** (device A), **PyPhPO** (device B), and **PyPhB** (device C) are depicted in Figure 8, and the corresponding key EL data are summarized in Table 3. As shown in Figure 7a and Figure S9, the device A based on **PyPhDPA** displayed an emission peaking at ca. 532 nm, which was red-shifted compared with the emission of **PyPhDPA** in 1.0 wt% doped PAMMA film and even broader than the emission of **PyPhDPA** in the THF/water mixture with f_{w} = 95%, indicating that the EL spectrum was composed of emissions mainly from aggregated **PyPhDPA** in the emissive layer (EML).[74] The morphology of **PyPhDPA**-doped TCTA film was then investigated with an atomic force microscope (AFM), which showed obvious aggregated particles with a large root-mean-square (RMS) roughness of 7.45 nm (Figure S10a). Therefore, the aggregation of **PyPhDPA** might lead to the insufficient energy transfer from the host to the complex, and thus caused a tiny emission from the TCTA host at ca. 390 nm.[46, 75] In addition, a weak emission peaking at around 450 nm was observed for device A, which was attributed to the exciplex emission from TAPC:TPBI.[76] Since the charge transport ability of TPBI [electron mobility of ~ 10^{-5} $\mathrm{cm^2/(V{\cdot}s)}$] is much weaker than that of TCTA [hole mobility of ~ 3×10^{-4} $\mathrm{cm^2/(V{\cdot}s)}$], the hole-electron recombination zone would be closer to the interface of TCTA/TPBI.[77] Moreover, as supported by the density−voltage curves of the single carrier devices based on TCTA film doped with 8 wt% of **PyPhDPA** (Figure S11), the much higher current density of the hole-only device than that of the electron-only device indicated that diphenylamino group would further promote the unbalanced electron-hole transport property. Therefore, together with the inefficient energy transfer within the EML mentioned above, the exciplex emission from TCTA:TPBI appeared. However, due to the relatively high PLQY (= 0.53) of **PyPhDPA** in the 8 wt% doped TCTA film, device A still showed decent EL efficiencies with the maximum EQE, CE, and PE of 10.5%, 34.3 cd $\mathrm{A^{-1}}$ and 30.3 lm $\mathrm{W^{-1}}$, respectively. Incorporation of the electron-withdrawing diphenylphosphino oxide group can effectively enhance the electron injection/transport ability of the resultant compounds to balance the hole-electron transport property within the EML.[78, 79] Therefore, probably because the recombination zone has been shifted closer to the center of EML due to the improved charge transport balance, which was evidenced by the density−voltage curves of the single carrier devices based on TCTA film doped with 8 wt% of **PyPhPO** (Figure S11), no exciplex emission from TCTA:TPBI emerged for **PyPhPO**-based device B. However, a tiny emission at ca. 390 nm from the TCTA host was still observed, indicating that the energy transfer from the host to the emitter was not complete. The incomplete energy transfer might result from the aggregate of **PyPhPO**, as supported by the red-shifted EL spectrum that displayed the enhanced emission with the peak at 524 nm and shoulder at 560 nm (Figure S9) and the AFM image for the **PyPhPO**-doped TCTA film (Figure S10b). Nevertheless, with improved charge balance and even higher PLQY (= 0.76) of **PyPhPO** in the 8 wt% doped TCTA film, device B showed much better performance with the peak EQE, CE, and PE increased to 16.8%, 62.0 cd A^{-1} and 52.3 lm W^{-1}, respectively. For the device C based on **PyPhB**, although the EL spectrum was broader than the PL spectrum of **PyPhDPA** in 1.0 wt% doped PAMMA film (Figure S9), it still displayed a nearly unshifted emission peak at 504 nm. This result implied that the aggregation of **PyPhB** in the EML has been effectively suppressed to some extent compared with the cases of **PyPhDPA** and **PyPhPO** in the corresponding EMLs, which had been confirmed by the much better morphology with small roughness (RMS = 0.62 nm) of **PyPhB**-doped TCTA film (Figure S10c). This result was reasonable because the dimesitylboryl group was larger than diphenylamino and diphenylphosphino oxide groups. In addition, as the density−voltage curves of the single carrier devices based on **PyPhB**-doped TCTA film (Figure S11) and previous studies revealed, the dimesitylboryl group had a strong π-electron accepting ability which can enhance the electron injection/transport property of the related emitters.[14, 80, 81] Therefore, the efficient energy transfer and more balanced charge transport within the EML could be expected, leading to the absence of both the exciplex emission from TCTA:TPBI and the emission from the TCTA host (Figure 8a). Besides, the TCTA film doped with 8 wt% **PyPhB** showed impressively high PLQY of 0.66. With all these advantages, device C gave the best performance with the maximum luminance (L_{max}), EQE, CE, and PE further increased to 15496 cd m^{-2}, 21.7%, 61.9 cd A^{-1} and 54.8 lm W^{-1}, respectively. To the best of our knowledge, the efficiencies of the device C based on **PyPhB** were among the highest ever reported for doped solution-processed OLEDs utilizing AIE-active phosphorescent emitters.[31-35, 82-87] These results demonstrated that the electronic property of substituents attached to the alkynyl ligands could exert great influence on the EL performance of related alkynyl ligand-containing Pt(II) complexes. With hole-transport-type materials as the host for OLEDs, bulky electron-withdrawing substituents will help to improve the hole-electron transport balance and facilitate the energy transfer by suppressing the molecular aggregation, and thereby benefit the EL performance.

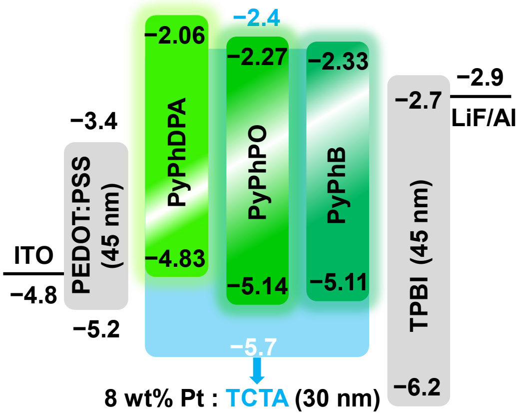

Figure 7. Device configuration and energy levels (eV) of the materials used in OLEDs.

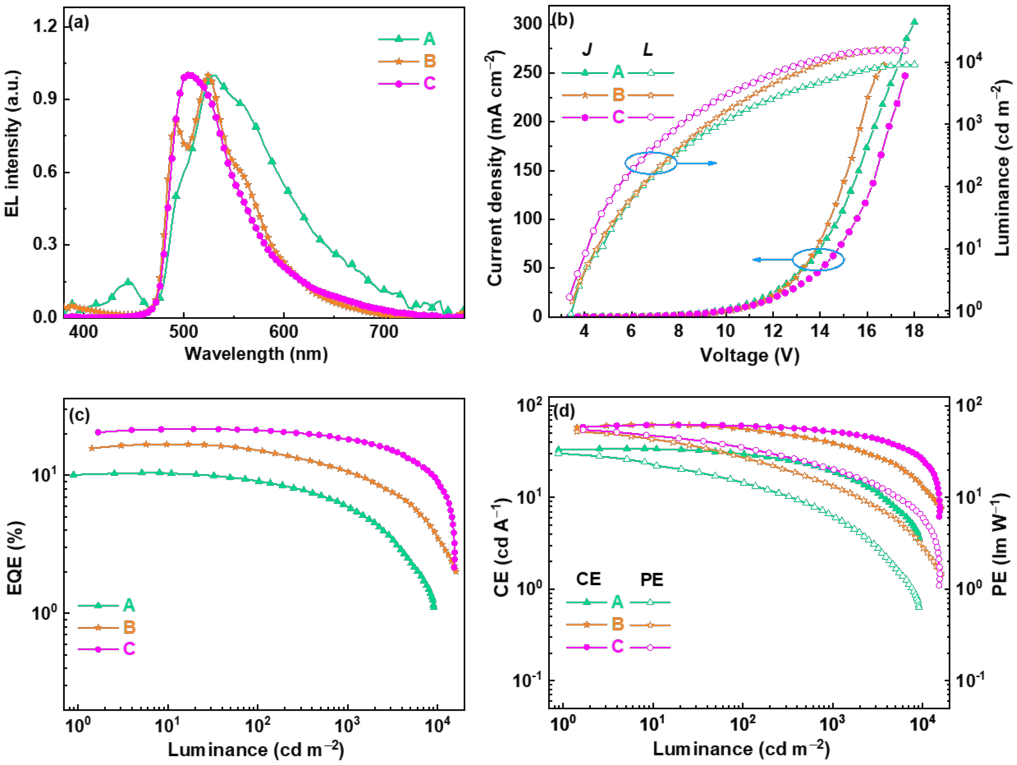

Figure 8. EL performance: a) EL spectra, b) curves of current density (*J*) – voltage (*V*) – luminance (*L*), c) curves of EQE vs luminance, and d) curves of CE and PE vs luminance.

Table 3. Key EL performance of all OLEDs based on the AIE-active Pt(II) complexes.

Device	Complex	λ_{EL} [nm]	$V_{turn\text{-}on}$ [a] [V]	L_{max} [cd m^{-2}]	EQE [b] [%]	CE [b] [cd A^{-1}]	PE [b] [lm W^{-1}]
A	**PyPhDPA**	532	3.5	9070	10.5/9.1	34.3/28.7	30.3/13.3
B	**PyPhPO**	524	3.3	15955	16.8/15.0	62.0/55.5	52.3/26.6
C	**PyPhB**	504	3.2	15496	21.7/21.0	61.9/60.4	54.8/34.5

[a] Driving voltage at *ca.* 1.0 cd m^{-2}. [b] The peak value/value at a luminance of 100 cd m^{-2}.

3. Conclusion

In summary, we developed a series of impressive AIE-active phosphorescent emitters by replacing one bidentate ligand of a conventional square-planar Pt(II) complex with two independent monodentate ligands. This strategy could provide more space for the coordination skeleton to deform from the planar configuration in the ground state to the quasi-tetrahedron configuration in the excited state, which led to the non-radiative decay and hence quite weak emissions of the resultant Pt(II) complexes in solutions. However, in the aggregate state, this crucial coordination skeletal deformation would be greatly restricted so that the related non-radiative decay rate constant was significantly decreased, resulting in intense emissions. On the basis of the experimental and theoretical calculation results, these newly developed Pt(II) complexes were typical AIE-active phosphorescent emitters, and the working mechanism of their AIE behaviors was mainly attributed to the restriction of coordination skeletal deformation. To further enhance the emissions in the aggregate state, strong-field ligands, i.e., alkynyl ligands, were used to raise the *d–d* state, leading to improved PLQYs of the resulting Pt(II) complexes in the solid state. Finally, solution-processed OLEDs were fabricated to evaluate the EL properties of the AIE-active Pt(II) complexes, which displayed outstanding device performance with the peak EQE, CE, and PE of 21.7%, 61.9 cd A^{-1}, and 54.8 lm W^{-1}, respectively, ranking them among the best AIE-active phosphorescent emitters for OLEDs. This work proposes a new mechanism, namely, restriction of coordination skeletal deformation (RCSD), to understand the AIE behaviors of Pt(II) complexes bearing two monodentate ligands, and thus opens up a myriad of possibilities for designing high performance AIE-active phosphorescent Pt(II) complexes. By delicately functionalizing the three ligands in this type of Pt(II) complexes with different substituents, we believe the resultant AIE-active phosphorescent emitters will have great potential for applications in not only highly efficient OLEDs but also high performance bioimaging and chemosensing systems. Furthermore, by considering the potential anti-cancer activity of Pt(II) complexes, AIE-active phosphorescent Pt(II) complexes may also have a promising application in biomedical theranostics.[88, 89]

Supporting Information

Supporting Information is available from the Wiley Online Library or from the author.

Acknowledgements

The authors gratefully acknowledge the financial support from the National Natural Science Foundation of China (21602170, 21875179, 51803163, 21572176, and 51873176), the Science, Technology and Innovation Committee of Shenzhen Municipality (JCYJ 20180507183413211), the Natural Science Foundation of Shaanxi Province (2019JZ-29 and 2019JQ-188), and Key Laboratory Construction Program of Xi'an Municipal Bureau of Science and Technology (201805056ZD7CG40). The characterization assistance from the Instrument Analysis Center of Xi'an Jiaotong University is also acknowledged. W.-Y. Wong thanks Hong Kong Research Grants Council (PolyU 153062/18P and C6009-17G), the Hong Kong Polytechnic University (1-ZE1C) and Ms Clarea Au (847S) for the financial support.

Conflict of Interest

The authors declare no conflict of interest.

Keywords

aggregation-induced emission, coordination skeletal deformation, emission mechanism, organic light-emitting device, phosphorescent Pt(II) complex

[1] J. Mei, N. L. Leung, R. T. Kwok, J. W. Lam, B. Z. Tang, *Chem. Rev.* **2015**, *115*, 11718.

[2] J. Luo, Z. Xie, J. W. Y. Lam, L. Cheng, H. Chen, C. Qiu, H. S. Kwok, X. Zhan, Y. Liu, D. Zhu, B. Z. Tang, *Chem. Commun.* **2001**, 1740.

[3] Y. Hong, J. W. Y. Lam, B. Z. Tang, *Chem. Soc. Rev.* **2011**, *40*, 5361.

[4] J. Mei, Y. Hong, J. W. Y. Lam, A. Qin, Y. Tang, B. Z. Tang, *Adv. Mater.* **2014**, *26*, 5429.

[5] Z. He, C. Ke, B. Z. Tang, *ACS Omega* **2018**, *3*, 3267.

[6] Y. Chen, J. W. Y. Lam, R. T. K. Kwok, B. Liu, B. Z. Tang, *Mater. Horiz.* **2019**, *6*, 428.

[7] Y. Li, S. Liu, T. Han, H. Zhang, C. Chuah, R. T. K. Kwok, J. W. Y. Lam, B. Z. Tang, *Mater. Chem. Front.* **2019**, *3*, 2207.

[8] S. Xu, Y. Duan, B. Liu, *Adv. Mater.* **2019**, *n/a*, 1903530.

[9] K. Kokado, T. Machida, T. Iwasa, T. Taketsugu, K. Sada, *J. Phys. Chem. C* **2018**, *122*, 245.

[10] H. Zhang, J. Liu, L. Du, C. Ma, N. L. C. Leung, Y. Niu, A. Qin, J. Sun, Q. Peng, H. H. Y. Sung, I. D. Williams, R. T. K. Kwok, J. W. Y. Lam, K. S. Wong, D. L. Phillips, B. Z. Tang, *Mater. Chem. Front.* **2019**, *3*, 1143.

[11] H. Qian, M. E. Cousins, E. H. Horak, A. Wakefield, M. D. Liptak, I. Aprahamian, *Nat. Chem.* **2017**, *9*, 83.

[12] Y. Gong, Y. Zhou, B. Yue, B. Wu, R. Sun, S. Qu, L. Zhu, *J. Phys. Chem. C* **2019**, *123*, 22511.

[13] Y. Tu, J. Liu, H. Zhang, Q. Peng, J. W. Y. Lam, B. Z. Tang, *Angew. Chem. Int. Ed.* **2019**, *58*, 14911.

[14] Z. M. Hudson, C. Sun, M. G. Helander, Y. L. Chang, Z. H. Lu, S. N. Wang, *J. Am. Chem. Soc.* **2012**, *134*, 13930.

[15] Y. Zhang, B. He, W. Luo, H. Peng, S. Chen, R. Hu, A. Qin, Z. Zhao, B. Z. Tang, *J. Mater. Chem. C* **2016**, *4*, 9316.

[16] K. Kokado, K. Sada, *Angew. Chem. Int. Ed.* **2019**, *58*, 8632.

[17] A. M'hamedi, M. A. Fox, A. S. Batsanov, H. A. Al-Attar, A. P. Monkman, M. R. Bryce, *J. Mater. Chem. C* **2017**, *5*, 6777.

[18] M. Xie, C. Han, Q. Liang, J. Zhang, G. Xie, H. Xu, *Sci. Adv.* **2019**, *5*, eaav9857.

[19] J.-X. Ru, L.-P. Guan, X.-L. Tang, W. Dou, X. Yao, W.-M. Chen, Y.-M. Liu, G.-L. Zhang, W.-S. Liu, Y. Meng, C.-M. Wang, *Inorg. Chem.* **2014**, *53*, 11498.

[20] H. Shi, H. Sun, H. Yang, S. Liu, G. Jenkins, W. Feng, F. Li, Q. Zhao, B. Liu, W. Huang, *Adv. Funct. Mater.* **2013**, *23*, 3268.

[21] Q. Zhao, X. Zhou, T. Cao, K. Y. Zhang, L. Yang, S. Liu, H. Liang, H. Yang, F. Li, W. Huang, *Chem. Sci.* **2015**, *6*, 1825.

[22] J. Qing, X.-K. Liu, M. Li, F. Liu, Z. Yuan, E. Tiukalova, Z. Yan, M. Duchamp, S. Chen, Y. Wang, S. Bai, J.-M. Liu, H. J. Snaith, C.-S. Lee, T. C. Sum, F. Gao, *Adv. Energy Mater.* **2018**, *8*, 1800185.

[23] Q. Zhao, F. Li, C. Huang, *Chem. Soc. Rev.* **2010**, *39*, 3007.

[24] Y. Chi, P.-T. Chou, *Chem. Soc. Rev.* **2010**, *39*, 638.

[25] C. Fan, C. Yang, *Chem. Soc. Rev.* **2014**, *43*, 6439.

[26] L. Wang, Z. Gao, C. Liu, X. Jin, *Mater. Chem. Front.* **2019**, *3*, 1593.

[27] L.-L. Wen, X.-G. Hou, G.-G. Shan, W.-L. Song, S.-R. Zhang, H.-Z. Sun, Z.-M. Su, *J. Mater. Chem. C* **2017**, *5*, 10847.

[28] H. Wu, T. Yang, Q. Zhao, J. Zhou, C. Li, F. Li, *Dalton Trans.* **2011**, *40*, 1969.

[29] J. Wu, Y. Li, C. Tan, X. Wang, Y. Zhang, J. Song, J. Qu, W.-Y. Wong, *Chem. Commun.* **2018**, *54*, 11144.

[30] L. Zhang, Y. Li, W. Che, D. Zhu, G. Li, Z. Xie, N. Song, S. Liu, B. Z. Tang, X. Liu, Z. Su, M. R. Bryce, *Adv. Sci.* **2019**, *6*, 1802050.

[31] P. Li, Q.-Y. Zeng, H.-Z. Sun, M. Akhtar, G.-G. Shan, X.-G. Hou, F.-S. Li, Z.-M. Su, *J. Mater. Chem. C* **2016**, *4*, 10464.

[32] Y. Li, D. P.-K. Tsang, C. K.-M. Chan, K. M.-C. Wong, M.-Y. Chan, V. W.-W. Yam, *Chem. Eur. J.* **2014**, *20*, 13710.

[33] J. Zhao, Z. Feng, D. Zhong, X. Yang, Y. Wu, G. Zhou, Z. Wu, *Chem. Mater.* **2018**, *30*, 929.

[34] Y. Sun, X. Yang, B. Liu, H. Guo, G. Zhou, W. Ma, Z. Wu, *J. Mater. Chem. C* **2019**, *7*, 12552.

[35] H.-T. Mao, Y. Cui, G.-F. Li, G.-G. Shan, Q.-Y. Zeng, F.-S. Li, Z.-M. Su, *J. Mater. Chem. C* **2019**, *7*, 13461.

[36] V. Sathish, A. Ramdass, P. Thanasekaran, K.-L. Lu, S. Rajagopal, *J. Photochem. Photobiol. C* **2015**, *23*, 25.

[37] L. Ravotto, P. Ceroni, *Coord. Chem. Rev.* **2017**, *346*, 62.

[38] P. Alam, C. Climent, P. Alemany, I. R. Laskar, *J. Photochem. Photobiol. C* **2019**, *41*, 100317.

[39] Q.-C. Zhang, H. Xiao, X. Zhang, L.-J. Xu, Z.-N. Chen, *Coord. Chem. Rev.* **2019**, *378*, 121.

[40] J. Song, M. Wang, X. Zhou, H. Xiang, *Chem. Eur. J.* **2018**, *24*, 7128.

[41] L. Qu, C. Li, G. Shen, F. Gou, J. Song, M. Wang, X. Xu, X. Zhou, H. Xiang, *Mater. Chem. Front.* **2019**, *3*, 1199.

[42] A. Tsuboyama, H. Iwawaki, M. Furugori, T. Mukaide, J. Kamatani, S. Igawa, T. Moriyama, S. Miura, T. Takiguchi, S. Okada, *J. Am. Chem. Soc.* **2003**, *125*, 12971.

[43] C.-H. Yang, Y.-M. Cheng, Y. Chi, C.-J. Hsu, F.-C. Fang, K.-T. Wong, P.-T. Chou, C.-H. Chang, M.-H. Tsai, C.-C. Wu, *Angew. Chem. Int. Ed.* **2007**, *46*, 2418.

[44] Z. M. Hudson, C. Sun, M. G. Helander, H. Amarne, Z.-H. Lu, S. Wang, *Adv. Funct. Mater.* **2010**, *20*, 3426.

[45] Z. M. Hudson, C. Sun, M. G. Helander, Y.-L. Chang, Z.-H. Lu, S. Wang, *J. Am. Chem. Soc.* **2012**, *134*, 13930.

[46] F. K.-W. Kong, M.-C. Tang, Y.-C. Wong, M.-Y. Chan, V. W.-W. Yam, *J. Am. Chem. Soc.* **2016**, *138*, 6281.

[47] F. K.-W. Kong, M.-C. Tang, Y.-C. Wong, M. Ng, M.-Y. Chan, V. W.-W. Yam, *J. Am. Chem. Soc.* **2017**, *139*, 6351.

[48] T.-Y. Li, J. Wu, Z.-G. Wu, Y.-X. Zheng, J.-L. Zuo, Y. Pan, *Coord. Chem. Rev.* **2018**, *374*, 55.

[49] P. K. Chow, G. Cheng, G. S. M. Tong, W. P. To, W. L. Kwong, K. H. Low, C. C. Kwok, C. Ma, C. M. Che, *Angew. Chem. Int. Ed.* **2015**, *54*, 2084.

[50] S. Reineke, K. Walzer, K. Leo, *Phys. Rev. B* **2007**, *75*, 125328.

[51] C. Adachi, M. A. Baldo, M. E. Thompson, S. R. Forrest, *J. Appl. Phys.* **2001**, *90*, 5048.

[52] W. Holzer, A. Penzkofer, T. Tsuboi, *Chem. Phys.* **2005**, *308*, 93.

[53] Q. Wang, I. W. Oswald, X. Yang, G. Zhou, H. Jia, Q. Qiao, Y. Chen, J. Hoshikawa-Halbert, B. E. Gnade, *Adv. Mater.* **2014**, *26*, 8107.

[54] C.-W. Hsu, Y. Zhao, H.-H. Yeh, C.-W. Lu, C. Fan, Y. Hu, N. Robertson, G.-H. Lee, X. W. Sun, Y. Chi, *J. Mater. Chem. C* **2015**, *3*, 10837.

[55] K.-H. Kim, J.-L. Liao, S. W. Lee, B. Sim, C.-K. Moon, G.-H. Lee, H. J. Kim, Y. Chi, J.-J. Kim, *Adv. Mater.* **2016**, *28*, 2526.

[56] K. Tuong Ly, R.-W. Chen-Cheng, H.-W. Lin, Y.-J. Shiau, S.-H. Liu, P.-T. Chou, C.-S. Tsao, Y.-C. Huang, Y. Chi, *Nature Photon.* **2017**, *11*, 63.

[57] X. Yang, H. Guo, X. Xu, Y. Sun, G. Zhou, W. Ma, Z. Wu, *Adv. Sci.* **2019**, *6*, 1801930.

[58] A. F. Rausch, L. Murphy, J. A. G. Williams, H. Yersin, *Inorg. Chem.* **2012**, *51*, 312.

[59] G. Cheng, S. C. F. Kui, W.-H. Ang, M.-Y. Ko, P.-K. Chow, C.-L. Kwong, C.-C. Kwok, C. Ma, X. Guan, K.-H. Low, S.-J. Su, C.-M. Che, *Chem. Sci.* **2014**, *5*, 4819.

[60] Z.-Q. Zhu, K. Klimes, S. Holloway, J. Li, *Adv. Mater.* **2017**, *29*, 1605002.

[61] J. Li, F. Liang, Y. Zhao, X.-Y. Liu, J. Fan, L.-S. Liao, *J. Mater. Chem. C* **2017**, *5*, 6202.

[62] M. Mao, J. Peng, T.-L. Lam, W.-H. Ang, H. Li, G. Cheng, C.-M. Che, *J. Mater. Chem. C* **2019**, *7*, 7230.

[63] W. H. Lam, E. S.-H. Lam, V. W.-W. Yam, *J. Am. Chem. Soc.* **2013**, *135*, 15135.

[64] J. Brooks, Y. Babayan, S. Lamansky, P. I. Djurovich, I. Tsyba, R. Bau, M. E. Thompson, *Inorg. Chem.* **2002**, *41*, 3055.

[65] J. Zhao, F. Dang, Z. Feng, B. Liu, X. Yang, Y. Wu, G. Zhou, Z. Wu, W.-Y. Wong, *Chem. Commun.* **2017**, *53*, 7581.

[66] E. S.-H. Lam, D. P.-K. Tsang, W. H. Lam, A. Y.-Y. Tam, M.-Y. Chan, W.-T. Wong, V. W.-W. Yam, *Chem. Eur. J.* **2013**, *19*, 6385.

[67] A. Y.-Y. Tam, W. H. Lam, K. M.-C. Wong, N. Zhu, V. W.-W. Yam, *Chem. Eur. J.* **2008**, *14*, 4562.

[68] J. Manna, K. D. John, M. D. Hopkins, *Adv. Organomet. Chem.* **1995**, *38*, 79.

[69] J. Kalinowski, V. Fattori, M. Cocchi, J. A. G. Williams, *Coord. Chem. Rev.* **2011**, *255*, 2401.

[70] P.-T. Chou, Y. Chi, M.-W. Chung, C.-C. Lin, *Coord. Chem. Rev.* **2011**, *255*, 2653.

[71] H. Na, Louise M. Cañada, Z. Wen, J. I-Chia Wu, T. S. Teets, *Chem. Sci.* **2019**, *10*, 6254.

[72] K. M.-C. Wong, M. M.-Y. Chan, V. W.-W. Yam, *Adv. Mater.* **2014**, *26*, 5558.

[73] S. Sasaki, S. Suzuki, W. M. C. Sameera, K. Igawa, K. Morokuma, G.-i. Konishi, *J. Am. Chem. Soc.* **2016**, *138*, 8194.

[74] A. Poloek, C.-T. Chen, C.-T. Chen, *J. Mater. Chem. C* **2014**, *2*, 1376.

[75] Y.-Y. Noh, C.-L. Lee, J.-J. Kim, K. Yase, *J. Chem. Phys.* **2003**, *118*, 2853.

[76] B. S. Kim, J. Y. Lee, *Adv. Funct. Mater.* **2014**, *24*, 3970.

[77] T.-H. Han, M.-R. Choi, C.-W. Jeon, Y.-H. Kim, S.-K. Kwon, T.-W. Lee, *Sci. Adv.* **2016**, *2*, e1601428.

[78] H.-T. Mao, C.-X. Zang, G.-G. Shan, H.-Z. Sun, W.-F. Xie, Z.-M. Su, *Inorg. Chem.* **2017**, *56*, 9979.

[79] R. Du, C. Duan, Y. Li, J. Zhang, C. Han, H. Xu, *Chem. Eng. J.* **2019**, *374*, 471.

[80] J. Huo, H. Wang, S. Li, H. Shi, Y. Tang, B. Z. Tang, *Chem. Rec.* **2019**, 10.1002/tcr.201900068.

[81] L. Chen, G. Lin, H. Peng, S. Ding, W. Luo, R. Hu, S. Chen, F. Huang, A. Qin, Z. Zhao, B. Z. Tang, *Mater. Chem. Front.* **2017**, *1*, 176.

[82] H. Wang, L. Xie, Q. Peng, L. Meng, Y. Wang, Y. Yi, P. Wang, *Adv. Mater.* **2014**, *26*, 5198.

[83] Q. Zhang, S. Sun, W. Liu, P. Leng, X. Lv, Y. Wang, H. Chen, S. Ye, S. Zhuang, L. Wang, *J. Mater. Chem. C* **2019**, *7*, 9487.

[84] Y. Li, Z. Xu, X. Zhu, B. Chen, Z. Wang, B. Xiao, J. W. Y. Lam, Z. Zhao, D. Ma, B. Z. Tang, *ACS Appl. Mater. Interfaces* **2019**, *11*, 17592.

[85] L. Yu, Z. Wu, G. Xie, C. Zhong, Z. Zhu, D. Ma, C. Yang, *Chem. Commun.* **2018**, *54*, 1379.

[86] H. Zhao, Z. Wang, X. Cai, K. Liu, Z. He, X. Liu, Y. Cao, S.-J. Su, *Mater. Chem. Front.* **2017**, *1*, 2039.

[87] H. Liu, J. Zeng, J. Guo, H. Nie, Z. Zhao, B. Z. Tang, *Angew. Chem. Int. Ed.* **2018**, *57*, 9290.

[88] L. S. Hollis, W. I. Sundquist, J. N. Burstyn, W. J. Heiger-Bernays, S. F. Bellon, K. J. Ahmed, A. R. Amundsen, E. W. Stern, S. J. Lippard, *Cancer Res.* **1991**, *51*, 1866.

[89] G. Jin, R. He, Q. Liu, M. Lin, Y. Dong, K. Li, B. Z. Tang, B. Liu, F. Xu, *Theranostics* **2019**, *9*, 246.

Efficient AIE-active Pt(II) complexes containing two independent monodentate ligands were developed based on a new working mechanism, namely, restriction of coordination skeletal deformation (RCSD). A solution-processed OLED based on the AIE-active Pt(II) complex displayed an outstanding performance with the peak EQE of 21.7%, ranking it among the best AIE-active phosphorescent emitters for OLEDs.